Original research

COPD basal cells are primed towards secretory to multiciliated cell imbalance driving increased resilience to environmental stressors

Mircea Gabriel Stoleriu [ID],[1,2] Meshal Ansari,[2] Maximilian Strunz,[2] Andrea Schamberger,[2] Motaharehsadat Heydarian [ID],[2] Yaobo Ding,[2] Carola Voss,[2] Juliane Josephine Schneider,[2] Michael Gerckens,[2,3] Gerald Burgstaller,[2] Alejandra Castelblanco [ID],[2] Teresa Kauke,[1] Jan Fertmann,[1] Christian Schneider,[1] Juergen Behr,[2,3] Michael Lindner,[4] Elvira Stacher-Priehse,[5] Martin Irmler,[6] Johannes Beckers,[6,7,8] Oliver Eickelberg,[2,9] Benjamin Schubert,[2,10] Stefanie M Hauck [ID],[11] Otmar Schmid,[2] Rudolf A Hatz,[1] Tobias Stoeger,[2] Herbert B Schiller,[2] Anne Hilgendorff[2,12]

ABSTRACT

Introduction Environmental pollutants injure the mucociliary elevator, thereby provoking disease progression in chronic obstructive pulmonary disease (COPD). Epithelial resilience mechanisms to environmental nanoparticles in health and disease are poorly characterised.

Methods We delineated the impact of prevalent pollutants such as carbon and zinc oxide nanoparticles, on cellular function and progeny in primary human bronchial epithelial cells (pHBECs) from end-stage COPD (COPD-IV, n=4), early disease (COPD-II, n=3) and pulmonary healthy individuals (n=4). After nanoparticle exposure of pHBECs at air–liquid interface, cell cultures were characterised by functional assays, transcriptome and protein analysis, complemented by single-cell analysis in serial samples of pHBEC cultures focusing on basal cell differentiation.

Results COPD-IV was characterised by a prosecretory phenotype (twofold increase in MUC5AC$^+$) at the expense of the multiciliated epithelium (threefold reduction in Ac-Tub$^+$), resulting in an increased resilience towards particle-induced cell damage (fivefold reduction in transepithelial electrical resistance), as exemplified by environmentally abundant doses of zinc oxide nanoparticles. Exposure of COPD-II cultures to cigarette smoke extract provoked the COPD-IV characteristic, prosecretory phenotype. Time-resolved single-cell transcriptomics revealed an underlying COPD-IV unique basal cell state characterised by a twofold increase in KRT5$^+$ (P=0.018) and LAMB3$^+$ (P=0.050) expression, as well as a significant activation of Wnt-specific (P=0.014) and Notch-specific (P=0.021) genes, especially in precursors of suprabasal and secretory cells.

Conclusion We identified COPD stage-specific gene alterations in basal cells that affect the cellular composition of the bronchial elevator and may control disease-specific epithelial resilience mechanisms in response to environmental nanoparticles. The identified phenomena likely inform treatment and prevention strategies.

WHAT IS ALREADY KNOWN ON THIS TOPIC

⇒ Specific environmental irritants such as fine particulate matters with a diameter ≤2.5 µm are known to induce epithelial cell damage, disruption of barrier integrity, as well as systemic cytotoxicity in chronic obstructive pulmonary disease (COPD).

WHAT THIS STUDY ADDS

⇒ The resilience of the secretory cells and vulnerability of the multiciliated cells towards environmental pollutants in end-stage COPD air–liquid interface (ALI) cultures are provoked by an altered basal cell state characterised by increased basement membrane (extracellular matrix) production as well as Wnt and Notch pathway activities that perturbs the secretory-multiciliated balance towards reduced multiciliogenesis.

HOW THIS STUDY MIGHT AFFECT RESEARCH, PRACTICE OR POLICY

⇒ Our study based on a physiological, long-term three-dimensional primary human bronchial epithelial cell culture model at ALI and validated by functional and structural compositional assays and multiomics analysis in vitro, enabled a realistic simulation of the pathophysiological changes provoked by environmental nanoparticle exposure in end-stage COPD, thereby informing prevention and therapy.

INTRODUCTION

In chronic obstructive pulmonary disease (COPD), the bronchial epithelium is continuously challenged by irritants inducing epithelial cell damage, disruption of barrier integrity and systemic cytotoxicity. Specifically, fine particulate matters ≤2.5 µm (PM$_{2.5}$)[1] such as respirable combustion-related

carbon black-like soot nanoparticles (CNPs) and occupationally relevant metal-based materials from industrial and heavily urbanised sites[2] such as zinc oxide (ZnO) provoke inflammatory and cytotoxic effects,[3 4] resulting in lung function decline and increased morbidity and mortality.[5] Counteracting the heterogeneous environmental challenges through highly specialised secretory and multiciliated cells, the mucociliary elevator defines the protective physical barrier of the bronchial epithelium. Specific regeneration of the damaged epithelium is guaranteed through basal stem cells, dictating secretory-multiciliated cell fate in nanoparticles (NPs) or cigarette smoke induced injury.[6] ZnO NPs induce short (Zn fever) and long-term toxicity (chemical pneumonitis, epithelial cell hyperplasia, pulmonary fibrosis)[7] and drive COPD progression[8] by reducing mucociliary clearance, and enhancing NP accumulation and translocation.[9] Chronic CNP exposure results in long-term effects, such as chronic airway inflammation and fibrosis.[10]

Whereas data on increased mortality and morbidity following short-term and long-term NP exposure are available,[8 11] pathomechanistic insight into NP effects that define the survival of airway lining cells and molecular changes to the basal stem cell population influencing regenerative capacities is missing in COPD.

We characterised the specific response of primary human bronchial epithelial cells (pHBECs) from end-stage COPD and non-chronic lung disease (non-CLD) proximal airways to environmentally relevant NP in a physiological long-term three-dimensional (3D) air–liquid interface (ALI) culture. We addressed submaximal doses of ZnO and compared the effects to the proinflammatory environmental irritants CNP and lipopolysaccharide (LPS), mimicking prevalent non-infectious and infectious causes of disease exacerbation. The use of a high-end aerosol-cell exposure system enabled us to delineate NP-induced effects on cell composition, function and transcription. We used single-cell analysis to clarify whether compositional and functional characteristics of COPD pHBEC cultures were driven by differences in cell frequencies and function.

Significantly adding to previous reports, our study addressed the healthy and diseased human bronchial epithelium in response to prevalent NPs in a clinically relevant, standardised fashion.[12] In addition, our study demonstrated increased resilience towards NP in end-stage COPD derived pHBEC cultures, which coincided with an increased ratio of secretory to multiciliated cells, and was successfully recapitulated in vivo. Important pathophysiological insight was provided by longitudinal single-cell analysis of basal cell differentiation in the ALI culture model, revealing a highly distinct COPD-associated state of the airway basal cell. Its characteristic increase in basement membrane (extracellular matrix) ECM production as well as Wnt and Notch pathway activities persists into differentiated progeny and perturbs the secretory-multiciliated balance towards reduced multiciliogenesis.

MATERIALS AND METHODS

For detailed protocols, please refer to online supplemental files 1 and 2.

Patient characteristics

Primary cultures were derived from thoracic surgery in age-matched and sex-matched COPD-IV (n=6), COPD-II (n=3, according to COPD classification of Global Initiative for Chronic Obstructive Lung Disease[13]) and patients without chronic lung disease (non-CLD, n=4) (Thoracic Surgery, LMU Hospital; Asklepios Medical Center Munich-Gauting; table 1, online supplemental figure 1).

Isolation and culture of pHBEC

pHBEC isolation: For exposure experiments, liquid nitrogen frozen pHBECs, isolated from proximal bronchial tissue (n=4 COPD-IV, n=3 COPD-II, n=4 non-CLD) with Pronase E (Type XIV, Sigma, REF:5147) digestion (20 hours, PneumaCult^M-Ex Plus Media (STEMCELL Technologies, REF:05041)), were restored and cultured.[14 15] DropSeq single-cell RNAseq analysis was performed in pHBECs isolated from fresh bronchial tissue (n=2 non-CLD, n=2 COPD-IV) by enzymatic Dispase dissociation (Protease from Bacillus polymyxa, SIGMA, D4818, REF:42613-33-2) (30 min, 37°C). Pronase digestion selects basal cells, whereas dispase digestion extracts basal, secretory and multiciliated cells. Both isolation protocols resulted in comparable cell ratios in culture.

pHBEC ALI culture: Isolated pHBECs were cultured in PneumaCultTM-Ex Plus Media (STEMCELL Technologies, REF:05041) on CollagenIV-coated transwell inserts until confluent before air-lift (ALI day 0/ALId0); basal medium supplemented PneumaCultTM (100x PneumaCultTM ALI Media, STEMCELL Technologies, REF:05006).

Ex vivo culture of bronchial punches at ALI: 4 mm punches were obtained from fresh bronchial tissue (PFM medical, Kai Europe, REF:48401) and cultured on transwells at ALI (PneumaCult).

Aerosolisation of NPS and pHBEC exposure

pHBECs (ALId30±2) were exposed to aerosolised CNPs (Printex 90; dose 10.8 cm²/cm²), ZnO NPs (low dose 0.14 cm²/

Table 1 Clinical characteristics of the COPD[13] patients included in the study

Pat. no	COPD stage	Sex	Pack-years	Smoker status	Surgery	FEV$_1$ (%)	CS	Heart disease
P1	IV	M	40	Ex	DLTX	13.2	Yes	No
P2	IV	M	30	Ex	SLTX	18.3	Yes	No
P3	IV	F	40	Ex	DLTX	14.8	Yes	No
P4	III-IV	M	15	Ex	DLTX	19.3	Yes	No
P5	IV	M	30	Ex	DLTX	48	Yes	No
P6	IV	M	40	Ex	DLTX	18.9	Yes	No
P7	II	M	40	Ex	LOB	70.6	No	Yes
P8	I-II	M	n.a.	Active	LOB	79	No	No
P9	II	F	80	Ex	PN	59	No	No

COPD, chronic obstructive pulmonary disease; CS, corticosteroids; DLTX, double LTX; F, female; FEV$_1$, forced expiratory volume in 1 s; LOB, lobectomy; LTX, lung transplantation; M, male; n.a., not available; Pat. No., patient number; PN, pneumonectomy; SLTX, single LTX.

Table 2 Characteristics of the nebulised nanoparticles (NPs)

Nebulised NPs	BET[51] (m²/g)	Median diameter (nm)	NP conc (mg/mL)	Mass dose (µg/cm²)*	Surface area dose cm²/cm²
Sham (water)	–	–	0	0	–
LPS (1 mg/mL)	–	–	1	0.70	–
CNP/Printex90	310	201±48	5	3.50	10.80
ZnO low dose	12	307±12	1.75	1.22	0.147
ZnO high dose	12	-†	38.12	26.70	3.20

Median diameter: volume-weighted median diameter (±SD, n=3) of size distribution of NP agglomerates in nebulised suspension measured by dynamic light scattering
*Cell delivered surface area dose is calculated from the product of the deposited NP mass per cell-covered area (µg/cm²) measured with a quartz crystal microbalance and the BET value of the NPs.
†NP concentration is too high for dynamic light scattering measurement.
BET, Brunauer, Emmett and Teller; CNPs, carbon nanoparticles; LPS, lipopolysaccharide ; ZnO, zinc oxide.

cm^2, high dose 3.19 cm^2/cm^2) and compared with an inflammatory (LPS, *Escherichia coli* O55:B5, 1 mg/mL; 0.699 µg/ cm^2) and an unchallenged control (saline solution 0.9%) for 24 hours (NP characteristics table 2). Uniform aerosol deposition of 200 µL suspension was achieved by ALICE CLOUD technology (VITROCELL CLOUD 12, VITROCELL Systems, Waldkirch, Germany, figure 1A).[16]

Cigarette smoke extract (CSE) exposure: CSE was added to the basal culture medium of COPD-II derived pHBECs (n=3).[15]

Functional analysis of pHBEC ALI cultures
Transepithelial electrical resistance (TEER, Ohm×1.12 cm^2) was performed as a measure of barrier cell integrity weekly (ALId7-28, reference in differentiated pHBECs: 950±250 Ohm×cm^2).[14 17]

WST-1 tetrazolium salt (WST) assay was performed according to the manufacturer's instructions (Roche Diagnostics, cell proliferation reagent WST-1, REF:11644807001, 05015944001) as a measure of metabolic cell viability on ALId28.

Lactate dehydrogenase (LDH) release was spectrophotometrically quantified at 490 nm via LDH Cytotoxicity Detection Kit (Roche Diagnostics, REF:11644793001)[14] on ALId28.

Ciliary velocity
Ciliary beating frequencies (CBF; 1920×1080 pixels at 50 fps; 3 videos >10 s) were recorded in ALI cultures (n=2 COPD-IV, n=2 COPD-II, n=2 non-CLD) using a computational video-processing pipeline applying a Discrete Fourier Transform to the signal intensity of 100 regions per frame (https://github.com/SchubertLab/ciliated_cells_video_analysis).[18]

RNA isolation and bulk transcriptome analysis
100 ng RNA (RNeasy Plus Mini Kit, Qiagen, Hilden, Germany) with high quality (Agilent 2100 Bioanalyzer, RNA Integrity >7) was amplified (WT PLUS Reagent Kit, Thermo Fisher Scientific, Waltham, USA). cDNA hybridisation (Human Clariom S arrays, Thermo Fisher Scientific) was followed by staining and scanning (GeneChip Scanner 3000 7G). Normalised SST-RMA gene-level data were obtained by Transcriptome Analysis Console (TAC; V.4.0.0.25; Thermo Fisher Scientific). Array data were submitted to the GEO database at NCBI (GSE208662).

DropSeq single-cell RNAseq analysis
DropSeq experiments were performed as described[19] with adaptations for single-cell library preparation[20] (online supplemental files 1 and 2). Serial single-cell RNA sequencing was performed for ALId0, 3, 5, 7, 14, 21, 28.

Quantitative proteomics: Liquid chromatography-mass spectrometry/ mass spectrometry of secretome samples
After washing (HBSS Ca^{2+}/Mg^{2+}) and filter-aided proteolysis with LysC and trypsin, proteins were analysed by mass spectrometry (QExactive HF, Thermo Fisher Scientific) coupled with UItimate 3000 RSLC nano-HPLC (Dionex)[21] by Proteome Discoverer (V.2.4 SP1, Thermo Fisher Scientific; V.2.4.1.15) for identification and quantification (Sequest HT search engine) using the SwissProt Human database (Release 2020_02, 20 435 sequences).

Immunofluorescence
Immunofluorescence (IF) was performed in ALId28 cultures (n=3 COPD-IV, n=3 COPD-II, n=3 non-CLD) using primary antibodies targeting secretory (goblet/ MU5AC$^+$, club/ CC10$^+$), multiciliated (Ac-Tub$^+$) and basal cells (KRT5$^+$, Laminin beta-3$^+$, RPLP$^+$, online supplemental files 1 and 2).[14] E-Cadherin and H&E stainings were analysed by optical microscopy in paraffin-embedded bronchial sections derived from n=2 COPD-IV and n=2 non-CLD patients.

Statistical analysis
Non-normal distributed data were represented as median and IQR. Wilcoxon rank test or Kruskal-Wallis test with Bonferroni post hoc analysis were used for group comparisons (GraphPad Prism V.8.2, San Diego, California, USA). CBF comparisons of top 10 regions with highest CBF (>1 Hz) per video were performed by Kolmogorov-Smirnov test after multiple testing adjustments by Benjamini-Hochberg corrections. Bulk transcriptome data were analysed using the environment R or CarmaWeb (for paired analyses). Genewise testing for differential expression used paired limma T-test. Gene sets were filtered using data-above-background p values<0.05 in at least 50% of the samples in at least one of the treatment groups per comparison. Sets of regulated genes were defined by raw p values<0.05 and filtered for fold change≥1.3. P values were adjusted for multiple testing (Benjamini-Hochberg corrections) where indicated. Pathway analysis by QIAGEN's Ingenuity Pathway Analysis (QIAGEN Redwood City, www.qiagen.com/ingenuity) used Fisher's exact test.

Secretome data were calculated by Student's t-test. P values were adjusted for multiple testing by Benjamini-Hochberg correction.

RESULTS
End-stage COPD shows increased resilience of bronchial airway epithelium towards cytotoxic NPs
We mimicked the exposure of the airway epithelium to cytotoxic NP by NP aerosolisation in pHBEC cultures from COPD-IV (n=4), COPD-II (n=3) and non-CLD (n=4) patients using the *VITROCELL CLOUD* exposure system (figure 1A). Environmentally abundant, low doses of ZnO (0.14 cm^2/cm^2) provoked cell damage-associated LDH release in non-CLD pHBECs together with a significant decrease in cell barrier integrity (figure 1B) in the presence of unaltered cell viability. In contrast, COPD-IV cultures exhibited significantly reduced effects of low dose ZnO
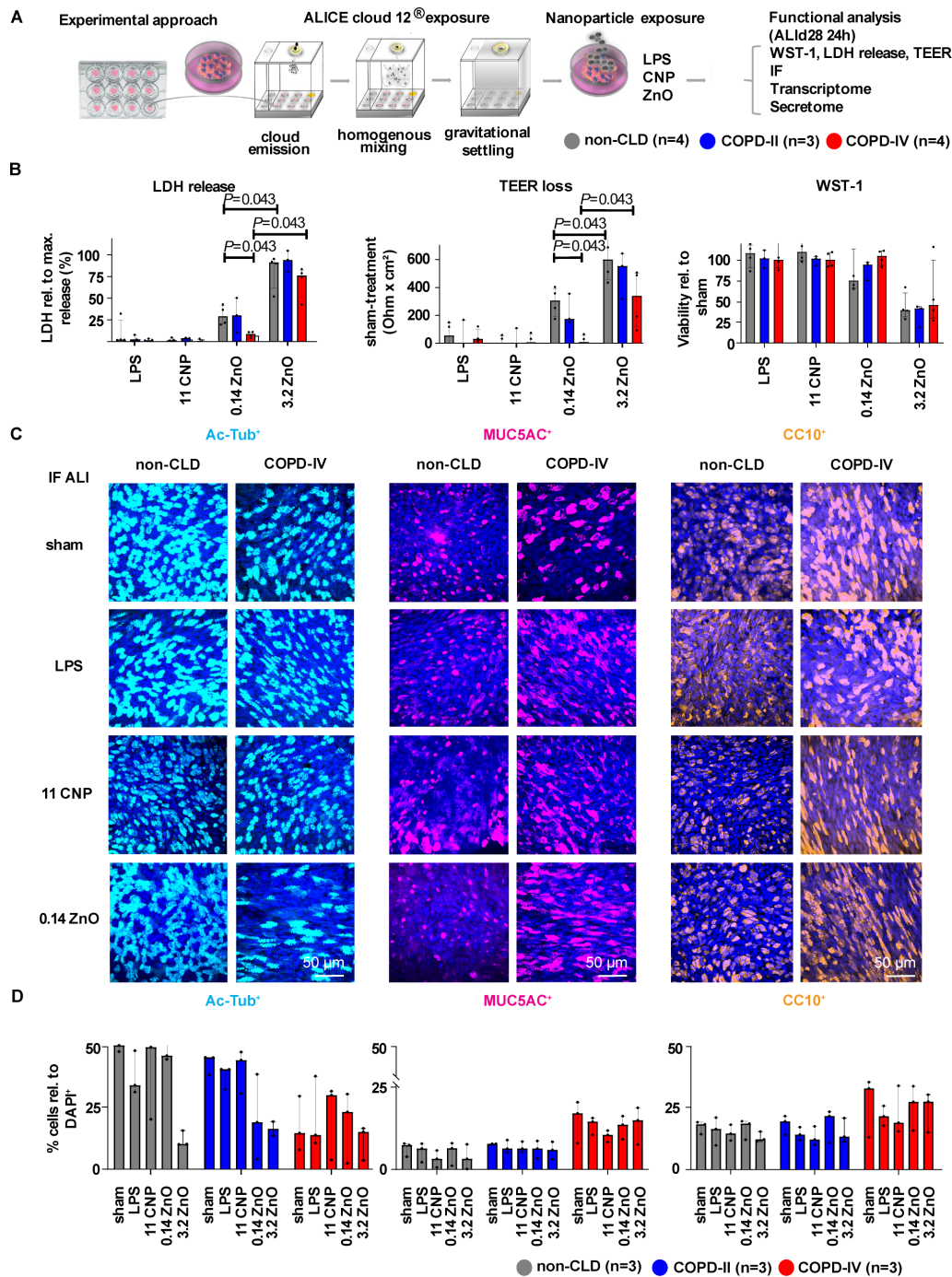
Figure 1 Increased resilience of COPD stage-IV derived pHBEC towards airborne toxin exposure associated with altered secretory to multiciliated cell balance at ALI. (A) Schematic representation of the experimental design demonstrating exposure of long-term ALI cultured pHBEC to environmentally relevant aerosolised cytotoxic (ZnO) and proinflammatory (CNP, LPS) nanoparticles (NP). (B) Analysis of membrane (left, lactate dehydrogenase (LDH) assay) and barrier (middle, transepithelial electrical resistance (TEER)) integrity and metabolic cell viability (right, tetrazolium salt assay (WST-1)) of pHBECs from non-CLD, COPD-II and COPD-IV patients 24 hours after NP exposure, showing a diminished susceptibility to ZnO exposure induced cellular damage indicated by reduced LDH release and cell barrier integrity loss as well as a preserved metabolic cell activity in COPD-IV cultures when compared with non-CLD and COPD-II cultures. Results are derived from n=4 non-CLD, n=3 COPD-II and n=4 COPD-IV pHBECs cultures and presented as median and IQR. (C, D) Exemplary images (three-dimensional microscopy) and quantification of confocal IF images of NP exposed pHBEC ALI cultures after antibody staining for secretory (MU5AC$^+$ and CC10$^+$) and multiciliated cells (Ac-Tub$^+$), showing an unchanged number of multiciliated cells in exposed non-CLD pHBECs, in contrast to a decrease in multiciliated cell number in COPD-II cultures and an unchanged number of secretory cells in both non-CLD and COPD-II pHBECs at ALId28. Results are derived from n=3 non-CLD, n=3 COPD-II and n=3 COPD-IV pHBEC cultures with IF quantification performed in 3–5 representative fields per transwell per condition (magnification ×63). Results are presented as median and IQR. Data information: Kruskal Wallis test with Bonferroni post hoc analysis was used for group comparisons. Results presented as median and IQR. Sham controls (saline solution 0.9%), LPS 1 mg/mL, CNP 10.8cm^2/cm^2, ZnO low dose 0.14 cm^2/cm^2 and ZnO high dose 3.19 cm^2/cm^2 at ALId30±2 after air-lift. Scale bar: 50 µm. ALI, air–liquid interface; CNP, carbon nanoparticle; COPD, chronic obstructive pulmonary disease; LPS, lipopolysaccharide; pHBEC, primary human bronchial epithelial cell.

exposure on LDH release and cell barrier integrity together with preserved metabolic cell activity (figure 1B).

These disease-grade-specific differences were recapitulated with high-dose exposure to ZnO NPs ($3.19\,cm^2/cm^2$) with an up to threefold increase in cell damage associated LDH release and a significant loss in membrane resistance (ΔTEER) in non-CLD pHBECs, whereas the effects on LDH release and ΔTEER were significantly reduced in COPD-IV pHBECs (figure 1B). Exposure to $3.19\,cm^2/cm^2$ ZnO resulted in reduced metabolic cell activity in all cultures (figure 1B).

Underlying the functional results, IF-based analysis showed strongest toxin effects in multiciliated cells in non-CLD and COPD-II cultures (figure 1C,D), whereas COPD-IV derived secretory cells were largely protected from these effects. Specifically, COPD-IV characteristic cell composition with the decreased multiciliated cell number and predominance of MUC5AC$^+$ and CC10$^+$ secretory cells remained unaffected (figure 1C,D).

In contrast to ZnO, exposure to LPS as a mimic of infectious exacerbations resulted in unchanged LDH release, barrier integrity and cell composition in pHBECs of all disease stages and non-CLD controls (figure 1B,C,D). Similar results were recapitulated on CNP exposure as a mimic of non-infectious exacerbations.

Altered cellular composition in end-stage COPD pHBECs coincided with disease-stage-specific changes in CBF. Whereas CNP or ZnO-exposed non-CLD multiciliated colonies conserved a physiological, biphasic CBF spectrum (7–16 Hz), COPD-IV pHBECs showed a loss in lower CBF (online supplemental figure 1).

Bulk transcriptome analysis of NP-exposed cultures confirmed 'classical' effects of ZnO, such as increased signalling in metal ion homoeostasis, mineral absorption and metal toxicity protecting metallothioneins (*MT1H, MT1F, MT1M, CKMT1B, MT1L, MT1P*) in COPD-IV and non-CLD cultures (online supplemental table 2, figure 2A). ZnO exposure in COPD-IV pHBECs resulted in the predicted activation of transcription factors driving a prosecretory phenotype (*SPDEF, FOXO1, IL-17C, PPRC1, RELA, LAMC1*, online supplemental table 3) in contrast to non-CLD cultures. ZnO exposure further provoked the pronounced activation of cilium assembly and movement genes in COPD-IV cultures in contrast to non-CLD (figure 2A, online supplemental figure 2). Mirroring the transcriptome changes, ZnO exposure resulted in the differential regulation of proteins involved in cilium biosynthesis, assembly, transport and movement in COPD-IV pHBECs (online supplemental tables 4 and 5, figure 2A). Comparative secretome analysis revealed regulation of common RNA-based enzymatic processes, organelle organisation, protein binding and biosynthesis in ZnO-exposed COPD-IV and non-CLD cultures (online supplemental table 5).

LPS exposure provoked an inflammatory response in non-CLD and COPD pHBECs (*CXCL1/2/3/5/6/8, TNF, VNN3*), orchestrated by *IL-17A*, associated with mucus hypersecretion and cilium movement (KEGG: hsa04657) and in line with the predicted activation of *TNF-α* and *IL-1ß* signalling. Enrichment analysis in non-CLD and COPD-IV cultures indicated the upregulation of innate defence mechanisms (eg, MHC class II complex, figure 2B,C). Analysis of non-CLD and COPD-IV revealed a comparable response with regard to the gene expression involved in NP clearance (figure 2C). Secretome analysis demonstrated significant regulation of proteins involved in cilium organisation and movement in LPS exposed COPD-IV cultures next to nonspecific protein and organelle biosynthetic processes (online supplemental table 6).

Prosecretory phenotype determines altered function of the airway epithelium in end-stage COPD

When investigating functional maturation of pHBECs in vitro, non-CLD and COPD-II cultures reached physiological TEER levels at ALId28 (740 ± 25 and 724 ± 240 Ohm$\times$cm^2), whereas COPD-IV cultures showed a 1.6-fold decrease in TEER values, indicating a substantial defect in barrier integrity (figure 3A), accompanied by altered ciliary function indicated by CBF analysis (online supplemental figure 1B).

Whereas non-CLD and COPD-II cultures showed a physiological number of multiciliated (Ac-Tub$^+$, 47%–49%) and secretory MUC5AC$^+$ and CC10$^+$ (6%–21%) cells at ALId28,[22] COPD-IV cultures were characterised by a threefold reduction in multiciliated and an increase in secretory MUC5AC$^+$ and CC10$^+$ cells (figure 3B). Reduced basal and suprabasal cell numbers, deducted through subtraction of secretory and multiciliated from total cells, suggest a differentiation defect in COPD-IV cultures (basal/suprabasal cells: 26% (non-CLD), 32% (COPD-II), 41% (COPD-IV)). We validated our culture conditions and confirmed the distribution of cell types observed in vitro in ex vivo bronchial punches, showing a homogeneous, ubiquitous distribution of multiciliated cells covered by a thin mucus film and a balanced distribution of secretory cells in non-CLD (online supplemental figure 3). In line with the in vitro results, IF in proximal bronchus sections for COPD-IV patients demonstrated misalignment of the bronchial epithelial layer in the presence of enlarged secretory cells (CC10$^+$ cells), abundant mucus production and the inhomogeneous distribution of multiciliated cells lacking a continuous cilia layer (figure 3C,D). These changes are closely matched by COPD-characteristic structural abnormalities including a thickened and irregular basement membrane, an increased number of secretory cells and reduced number of multiciliated cells (figure 3E) together with an altered CBF (figure 3F) in comparison to non-CLD airways.

Changes in COPD-IV cultures were partially mirrored in COPD-II pHBECs demonstrating lower multiciliated cell numbers at ALId28 when compared with non-CLD (figure 3A,B). Exposure of COPD-II pHBECs to CSE provoked phenotype progression showing a 1.4–1.6 fold reduction of multiciliated cells and a reduction in barrier integrity as compared with untreated COPD-II and non-CLD ALId28 cultures (figure 3A,B), whereas secretory cell numbers remained unchanged.

Bulk transcriptomics demonstrated an over-representation of carbohydrate/glycosaminoglycan metabolism in unexposed COPD-IV pHBECs together with a regulation of primary ciliogenesis and centrosome duplication genes (eg, Sirtuin, PTEN pathways, actin signalling, online supplemental figure 4, online supplemental table 7). Concomitant with the decrease in membrane integrity, we observed a significant activation of transmembrane carbohydrate and lipid metabolic processes, as well as genes engaged in cellular (de)differentiation, epithelial-to-mesenchymal transition (EMT) and ECM production (*TGF-ß1, XBP1, HIF-1A, FOXC1, FN1*) in unexposed COPD-IV cultures, confirmed by upstream regulator analysis (online supplemental table 8).

Secretome analysis of unexposed COPD-IV cultures revealed ubiquitous organelle organisation as well as common protein metabolic processes, together with regulation of proteins engaged in stem cell maintenance and differentiation, tight junction assembly as well as cilium assembly and Notch signalling in COPD-IV pHBECs, reflecting on secretory-multiciliated-cell differentiation (online supplemental table 9).
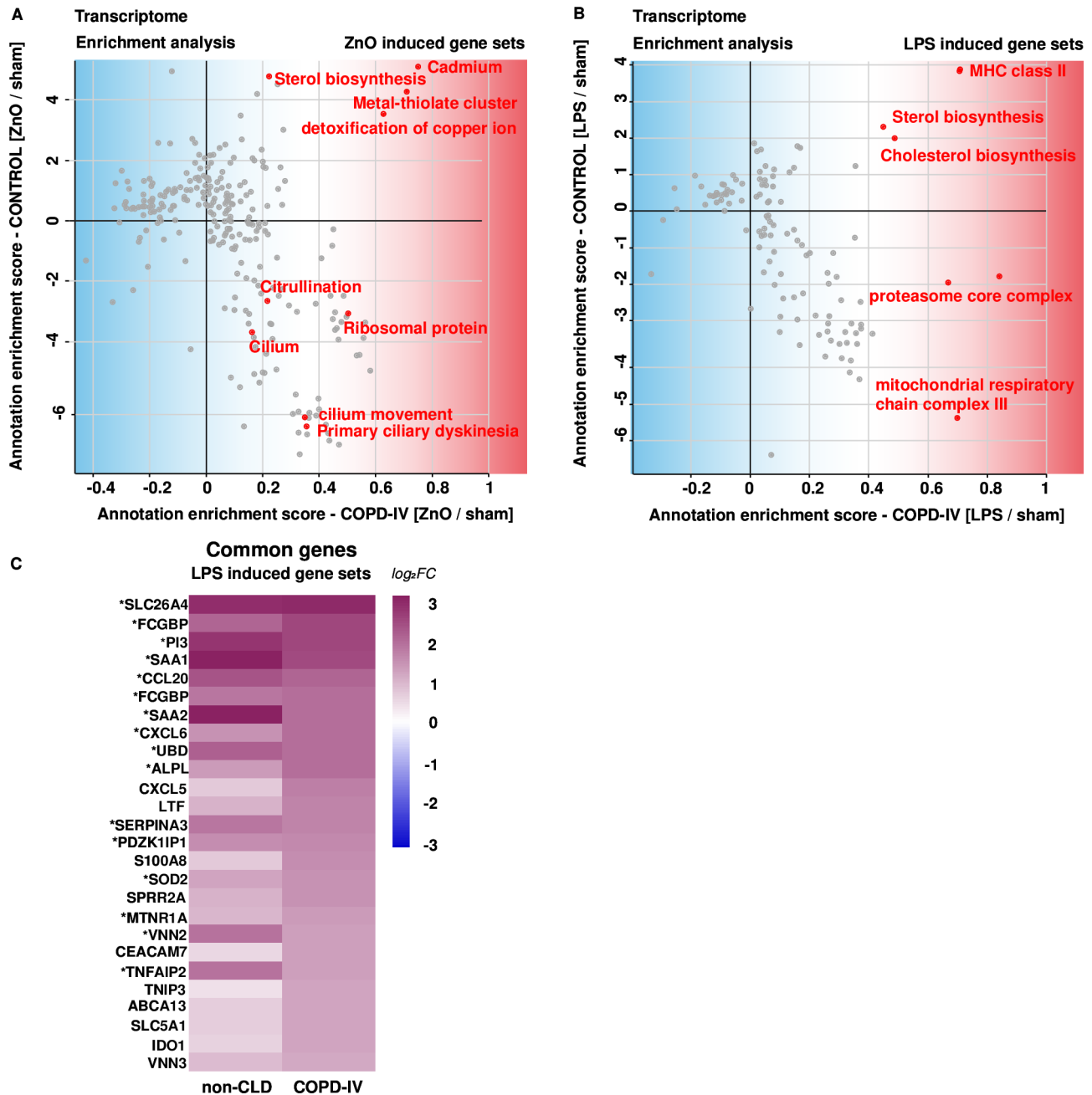
Figure 2 Healthy and diseased ALI cultures reveal shared gene expression and pathway regulation on LPS and ZnO exposure. (A) Pathway enrichment analysis from bulk transcriptome of non-CLD controls and COPD-IV ALI cultures, showing the presence of cilium regulation mechanisms in COPD-IV cultures on low-dose ZnO exposure. (B) Upregulation of innate defence mechanisms in both healthy and diseased ALI cultures in response to LPS exposure. (C) The heatmap illustrates the top 25 significantly upregulated genes from bulk transcriptome analysis of the LPS-exposed non-CLD and COPD-IV ALI cultures. Gene expression indicates a comparable response with regard to nanoparticle clearance. Genes with adjusted p values<0.1 are marked with an asterisk. Data information: Regulated genes were filtered by using raw p values<0.05 and FC (fold change) ≥1.3. $\log_2$FC are shown. Bulk transcriptome analysis was derived from n=3 non-CLD and n=3 COPD-IV pHBEC cultures. ALI, air–liquid interface; CLD, chronic lung disease; COPD, chronic obstructive pulmonary disease; LPS, lipopolysaccharide; pHBEC, primary human bronchial epithelial cell.

Longitudinal single-cell RNA-seq analysis revealed novel basal cell states in COPD giving rise to altered progeny of the airway epithelium

In order to understand the molecular underpinnings of the observed multiciliated to secretory cell imbalance and possible differentiation defect in COPD-IV cultures, we performed longitudinal single-cell RNA-seq analysis at 7 ALI culture time points (n=2 non-CLD, n=2 COPD-IV) (figure 4A). Single-cell clusters showed distinct gene expression profiles with culture

time point, disease state and cell type identity as explanatory variables (figure 4B,C). We annotated cell type identities based on published canonical marker genes and identified two types of basal stem cells (KRT5+/TRP63+), suprabasal cells (SERPINB4+), secretory cells (SCGB3A1+) and multiciliated cells (FOXJ1+). We also observed a prominent transitional cell state that was characterised by coexpression of secretory and multiciliated cell marker genes, indicating differentiation from secretory towards multiciliated cell identity, in line with the current model of
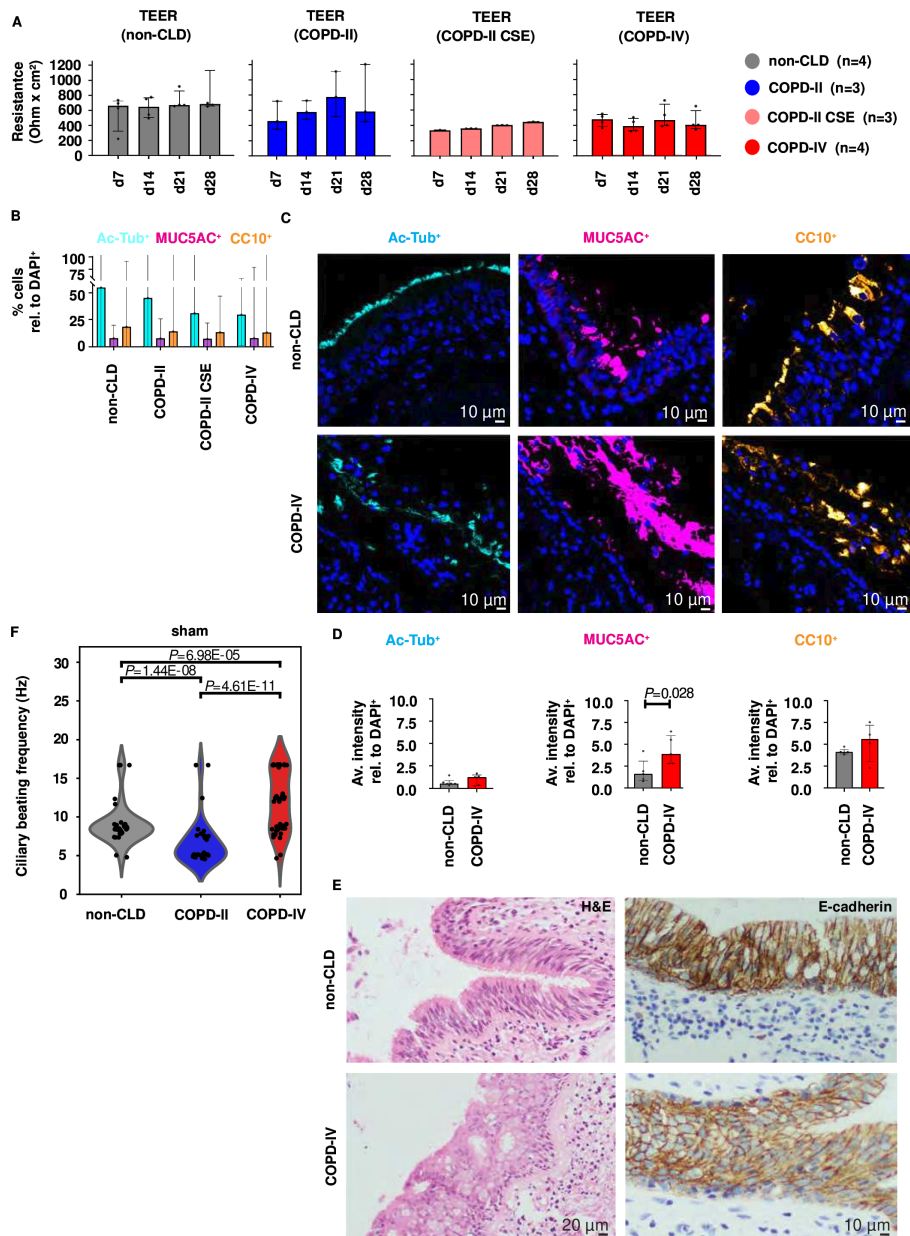
Figure 3 Altered cell differentiation in COPD stage-IV derived pHBEC at ALI resulted from basal cells imbalance. (A) Analysis of epithelial barrier integrity via transepithelial electrical resistance (TEER) of pHBEC isolated from non-CLD, COPD-II (native and+CSE) and COPD-IV patients, showing slightly reduced TEER values in COPD-II CSE when compared with the untreated COPD-II cultures. Results are derived from n=4 non-CLD, n=3 COPD-II, n=3 COPD-II CSE and n=4 COPD-IV pHBEC cultures. (B) Quantification of confocal three-dimensional IF microscopy of non-CLD, COPD-II, COPD-II CSE and COPD-IV derived pHBECs at ALId28 demonstrating a decrease in the number of multiciliated (Ac-Tub+) of COPD-II treated cultures vs untreated COPD-II and non-CLD cultures at ALId28. Secretory cell number remained almost unchanged on CSE exposure. The remaining cells from the total number of cells at ALId28 reflect the number of basal and suprabasal cells on the end-differentiated ALI cultures. Results are derived from n=3 non-CLD, n=3 COPD-II, n=3 COPD-II CSE and n=3 COPD-IV pHBEC cultures with IF quantification performed in 3–5 representative fields per condition. (C) IF microscopy of confocal IF images in sections of native bronchial tissue samples from n=2 COPD-IV and n=2 non-CLD patients (magnification ×20). (D) Quantification of confocal IF images in sections of native bronchial tissue samples from COPD-IV and non-CLD patients demonstrating the reduced presence of multiciliated (Ac-Tub+) cells and the dominant presence of MU5AC+ and CC10+ epithelial cells in COPD-IV cultures. Results are derived from n=2 non-CLD and n=2 COPD-IV pHBEC cultures with IF quantification performed in 3–5 representative fields per condition. (E) Optical microscopy of paraffin-embedded bronchial sections derived from n=2 COPD-IV and n=2 non-CLD patients stained with H&E as well as E-cadherin, showing an irregular and thicker basement membrane, more secretory cells and less multiciliated cells in COPD-IV in comparison to the non-CLD samples (magnification ×20). (F) Ciliary beating frequency (CBF, Hz) in non-CLD, COPD-II and COPD-IV derived pHBEC cultures at ALId28+1, at baseline level, demonstrating an altered, biphasic CBF pattern in COPD-IV with (aberrantly) slow and fast beating multiciliated cells and a physiological CBF between 7 and 16 Hz in non-CLD and COPD-II cultures. Results are derived from n=2 non-CLD, n=2 COPD-II and n=2 COPD-IV cultures at baseline level. Data information: Results presented as median and IQR. Comparative analysis for IF quantification of native bronchial tissue samples was performed by Wilcoxon test; and for CBF by Kolmogorov-Smirnov test adjusted by Benjamini-Hochberg test for multiple testing correction. Scale bar: 10 μm/20 μm. ALI, air–liquid interface; CLD, chronic lung disease; COPD, chronic obstructive pulmonary disease; CSE, cigarette smoke extract; pHBEC, primary human bronchial epithelial cell.
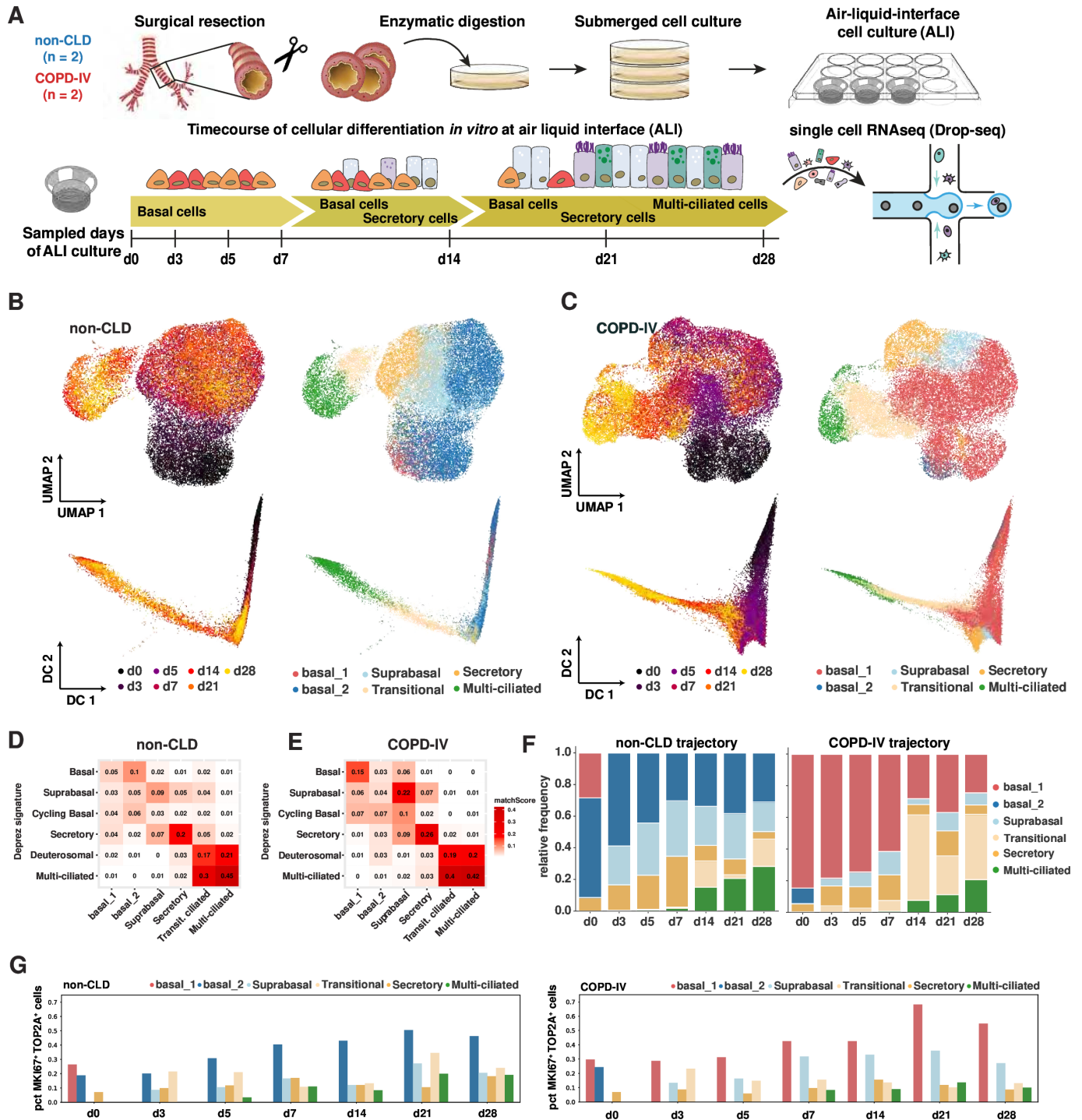
Figure 4 Longitudinal single-cell RNA-seq reveals altered differentiation dynamics in COPD-IV derived ALI cultures (n=2) in comparison to the non-CLD ALI cultures (n=2). (A) Schematic representation of the experimental design: ALI culture of pHBECs derived from n=2 non-CLD and n=2 COPD-IV patients followed by serial sampling and single-cell RNA-seq (Drop-seq) analysis on ALId0, 3, 5, 7, 14, 21, 28. (B, C) The indicated colour codes on UMAP and diffusion map (DC) embeddings show time points of sampling and cell type annotations for non-CLD control pHBEC B) and COPD-IV C) cultures. (D, E) The matchScore coefficients indicate the transcriptional similarity of cell type annotations in the pHBEC cultures to a in vivo single-cell RNA-seq reference dataset obtained from healthy individuals.[25] (F) The stacked bar graph shows changes in relative proportions of cell types generated in the pHBEC cultures at the indicated time points. (G) The bar graphs show the percentage of proliferating cells ($MKI67^+/TOP2A^+$) in the indicated experimental conditions and cell types. Data information: Results are derived from n=2 non-CLD and n=2 COPD-IV immediately processed pHBEC cultures following dispase dissociation protocol. Wilcoxon rank-sum test, Bonferroni corrected. ALI, air–liquid interface; CLD, chronic lung disease; COPD, chronic obstructive pulmonary disease; pHBEC, primary human bronchial epithelial cell.

human airway lineage hierarchy.[23 24] The transition state was positioned between secretory and multiciliated cell populations in UMAP embedding and diffusion maps of gene expression space, appearing mainly from ALId14 onwards (figure 4B,C).

In systematic comparisons, cell populations in single-cell data showed high matching scores with the single-cell atlas of healthy human airways[25] and a comprehensive description of the tracheal epithelium in never smokers and active smokers.[26] The correlation of marker genes of the in vitro model and in vivo cell type identities was highest with the matched cell type labels, indicating correct generation of in vivo like cell type identities in non-CLD and COPD-IV pHBECs (figure 4D,E, online supplemental figure 5).

Interestingly, basal stem cell states in control and COPD-IV pHBECs were highly distinct with a mixture of two cell states, further referred to as basal_1 and basal_2 at ALId0. The basal_1 cell state was predominantly present in COPD-IV samples, whereas the basal_2 state mostly appeared in non-CLD pHBECs with this difference persisting until ALId28. Suprabasal and secretory phenotypes occurred early (ALId3-7), followed by the appearance of multiciliated cell identities from ALId14 onwards (figure 4F). Notably, the difference in basal stem cell identity did not result in significant changes to proliferation capacity or differentiated progeny (figure 4G), but the accumulation of transitional cell states resulted in reduced proportions of multiciliated cell identities in COPD-IV cultures, indicating defective terminal differentiation into multiciliated cells (figure 4F).

Disease-associated alterations in basal stem cells are propagated into differentiated progeny

Conserved gene expression differences between basal_1 and basal_2 were identified by differential gene expression analysis for basal cells (ALId0, ALId28) (figure 5A,B), complementing genes that significantly distinguished the two basal cell states at the time points (figure 5C,D). During early time points, gene set enrichment analysis demonstrated basal_1 cells (dominant in COPD-IV) feature higher levels of basement membrane ECM components, as well as genes involved in Wnt and Notch signalling (figure 5E), in line with the bulk transcriptome data (online supplemental tables 10 and 11). Basal_2 cells (dominant in non-CLD) were characterised by increased expression levels for ribonucleoprotein complex, mitochondrial respiratory chain complex and tricarboxylic acid cycle (figure 5E,I).

In accordance with single-cell data, the number of $KRT5^+$/$LAMB3^+$ high basal_1 cells was significantly increased in native bronchi from the same COPD-IV patients when compared with non-CLD, whereas cells with the ribosomal protein $RPLP1^+$, a marker for basal_2 cells, decreased in COPD-IV when compared with non-CLD (online supplemental figure 6).

Differences between the basal_1 and basal_2 cell states suggest epigenetic differences in COPD-IV and non-CLD derived pHBECs as the variant histone H3 (*H3F3A*), representing an epigenetic imprint of transcriptionally active chromatin,[27] was predominantly expressed in non-CLD-derived basal cells and their differentiated progeny, that is, secretory and multiciliated cells (figure 5C,D). Systematic differential gene expression analysis for each cell type identified 11 upregulated and 177 down-regulated genes that were passed on from basal stem cells to their differentiated progeny (higher in COPD-IV; figure 5F,G), next to genes that were conserved in all cell types (figure 5H). The conserved changes were reflected by gene set and pathway enrichment analysis demonstrating decreased expression of the cytosolic ribosomal machinery in COPD-IV basal cells

(basal_1) to be conserved in all cell types during differentiation (figure 5I). Conversely, increased gene expression of the Notch pathway in COPD-IV, most notably Jagged-2 (*JAG2*), was propagated from basal_1 to secretory cells (figure 5C,J), through its impact on silencing the multiciliated gene programme[28] potentially explaining the observed defect in terminal differentiation in COPD-IV pHBECs (figure 4). In line with these findings, an increased activation of Notch signalling in COPD-IV cultures was found on bulk transcriptome analysis (online supplemental tables 10 and 11).

Further, Wnt signalling was significantly enriched in COPD-IV-associated basal_1 cells and their secretory cell progeny (figure 5K), in accordance with the ingenuity enrichment analysis derived from bulk transcriptome in untreated COPD-IV cultures (ie, *SOX4, SOX8, TLE1, WNT10B, WNT5A, WNT7B, WNT9B*; $-\log_{10}$(p value)=1.82).[29 30] ZnO exposure further induced engagement of Wnt signalling (*ie, AKT3, ALPL, BAD, BMP2, BMPR1A, CSF1, FZD10, LEF1, NAIP, SFRP4, TNFRSF1B, TNFSF11, WIF1, WNT5A, WNT5B*; $-\log_{10}$(p value)=2.46, online supplemental table 11), contributing to dysregulated secretory-multiciliated cell differentiation in line with previous studies.[31] This included pathways in close relation to Wnt signalling (*TGF-ß3, TGF-ßR2, IL1F10, IL1RAPL2, IL1RN, IL36G, SMAD9*).

Notch pathway-associated imbalance of multiciliated and secretory cell programmes in COPD

We quantified disease-associated changes in the secretory and multiciliated cell populations using marker gene expression profiles of airway epithelial cells in the healthy airway single-cell atlas.[25] The in vivo multiciliated gene signature scored highest in the pHBEC multiciliated cell population. COPD-IV pHBECs scored significantly lower for the in vivo multiciliated signature, particularly at earlier time points (figure 6A), whereas the in vivo secretory cell signature scored higher in COPD-IV pHBECs (figure 6B). The imbalanced multiciliated and secretory cell programme was also evident when quantifying individual marker genes such *TUBA1A* (multiciliated cells), *SCGB1A1* (secretory club cells) and *MUC5B* (secretory mucous cells) at the different time points (figure 6C). While disease-associated differences in basal stem cells (eg, *LGALS7, LAMB3*) persisted over time, we observed a gradual increase in secretory and multiciliated cell marker gene expression in non-CLD pHBECs (figure 6C). These results are in line with relative cell frequency reported in non-CLD ALI cultures showing a steady, threefold increase in the number of multiciliated cells over time (ALId14: 17.9%±5.1%, ALIdd28: 52.9%±1.2%), whereas secretory cell number peaked at ALId14 ($MUC5AC^+$ 10.2%±0.2%, $CC10^+$ 17.3%±0.7%), followed by decreased ($MUC5AC^+$, 5.4%±1%) or unchanged ($CC10^+$, 15%±5.3%) secretory cell frequencies until ALId28 (online supplemental figure 7). The secretory and multiciliated cell marker gene expression observed in non-CLD pHBECs was inversely regulated in COPD-IV samples and accompanied by a strong increase in Notch pathway activity, in particular from ALId14 onwards (figure 6D,E).

DISCUSSION

The continuous challenge of the proximal bronchial epithelium by environmental pollutants largely impacts on lung health, especially when epithelial regeneration capacity is exhausted such as in end-stage COPD.[32] Although contribution of $PM_{2.5}$ to COPD progression has been demonstrated,[8] underlying molecular mechanisms remain elusive in contrast to studies focusing
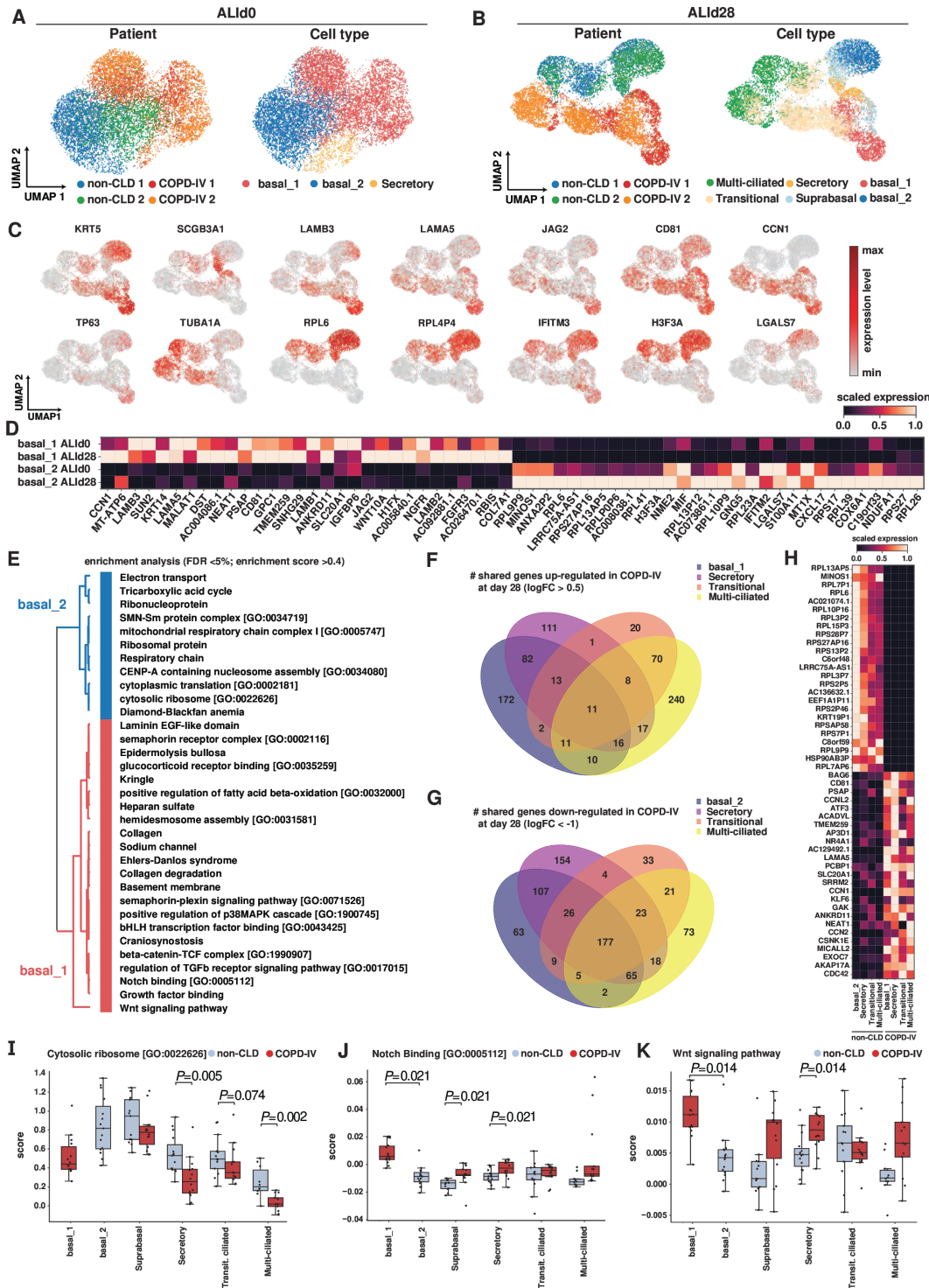
Figure 5 An altered basal cell state in ALI COPD-IV pHBECs propagates into its differentiated progeny. (A, B) UMAP embedding overlaid with sample identifier and cell type annotation for starting cells at ALId0 A) and endpoint of the differentiation at ALId28 B) for patients from both health conditions. (C) Feature plots of common marker genes of airway epithelial populations to confirm cell type labels at ALId28. Selected genes distinguishing the two basal populations (basal_1 for COPD-IV or basal_2 for non-CLD cultures). (D) Top 30 upregulated genes in either basal_1 or basal_2 population derived from differential tests between basal_1 and basal_2 cells. Genes that were significantly regulated on both ALId0 and 28 cells are shown. (E) Significantly enriched terms in the basal_1 and basal_2 signature (false discovery rate/FDR<0.05). (F, G) Venn-diagrams summarising the number of overlapping genes that were upregulated (F) or downregulated (G) at ALId28 COPD-IV cultures per cell type compared with non-CLD cultures. (H) Heatmap reflecting top 30 consistently upregulated and downregulated genes in COPD-IV in all cell populations at ALId28. Results are based on differential tests between COPD-IV and non-CLD for each cell type separately. (I–K) Boxplots showing the enrichment of gene signatures for the GO Terms 'cytosolic ribosome' (I), 'Notch binding' (J) and the UniProt keyword 'Wnt signalling pathway' (K) split by health status. Data information: Results are derived from n=2 non-CLD and n=2 COPD-IV immediately processed pHBEC cultures following dispase dissociation protocol. Wilcoxon rank-sum test, Bonferroni corrected. ALI, air–liquid interface; CLD, chronic lung disease; COPD, chronic obstructive pulmonary disease; pHBEC, primary human bronchial epithelial cell.
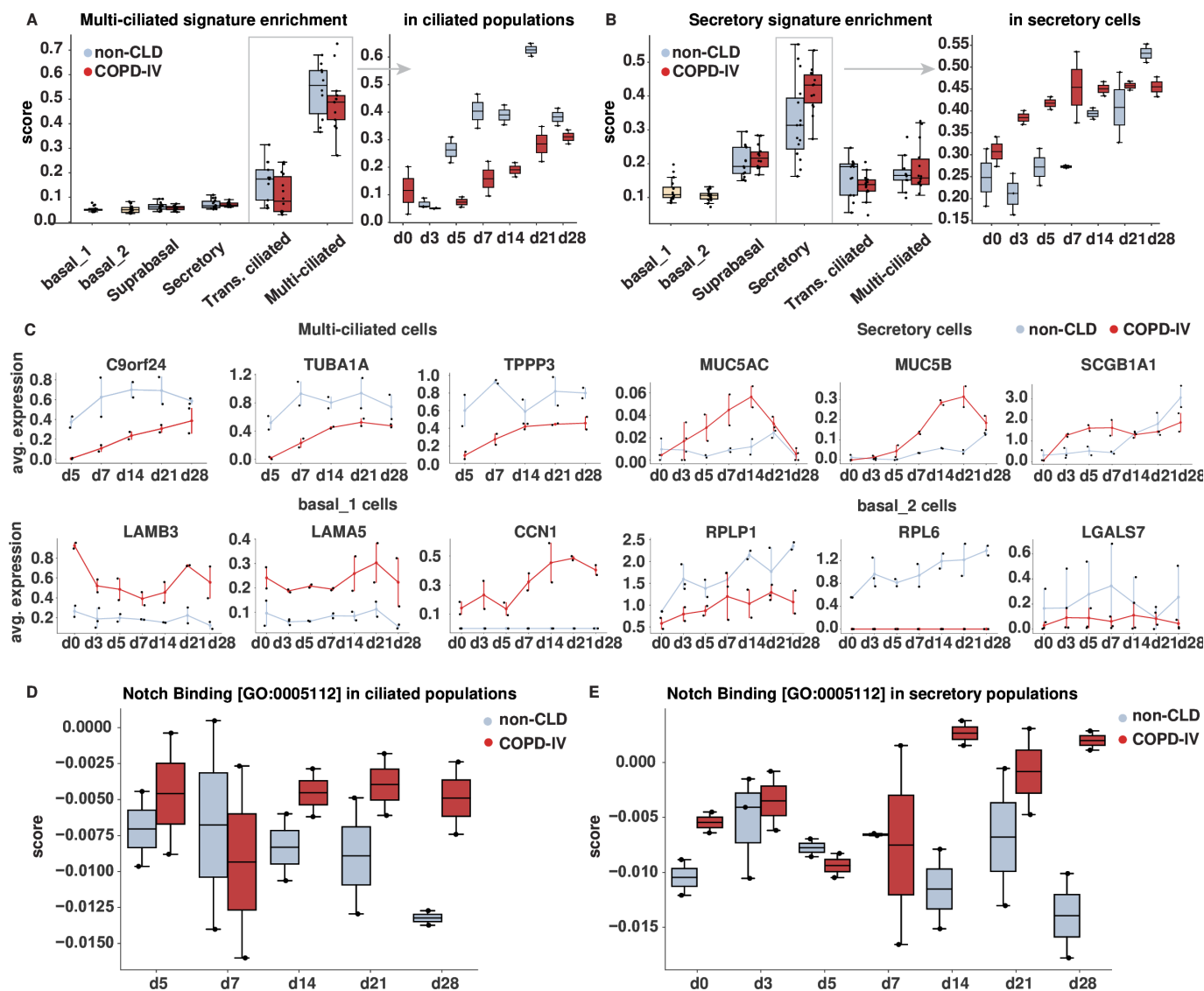
Figure 6 Altered secretory to multiciliated cell balance in COPD-IV-derived pHBECs is associated with increased Notch pathway activity. (A, B) Boxplots showing the enrichment of the multiciliated (A) and secretory (B) cell type signature[25] split by health status. Time points are pooled for all cell types, and progression of score over time is highlighted in relevant cell populations as indicated. (C) Gene kinetics of cell type markers for basal cells, multiciliated cells and secretory cells over the course of the experiment revealing disease-induced shifts propagated over time. (D, E) Boxplots summarising enrichment scoring results based on genes associated with the GO term 'Notch binding' over time, shown for only multiciliated (D) and secretory cells (E) separately. Data information: Results are derived from n=2 non-CLD and n=2 COPD-IV immediately processed pHBEC cultures following dispase dissociation protocol. Wilcoxon rank-sum test, Bonferroni corrected. CLD, chronic lung disease; COPD, chronic obstructive pulmonary disease; pHBEC, primary human bronchial epithelial cell.

on cigarette smoke induced basal cell damage and impaired cell differentiation.[15]

Increasing pathophysiological insight, we described the effects of prevalent environmental pollutants in 3D biomimetic end-stage COPD and non-CLD derived pHBEC ALI cultures (online supplemental figure 8) and delineated NP effects on cellular composition and function. In response to prevalent airborne irritants, we discovered the predominant survival of secretory cells in pHBEC cultures together with significant functional changes, that is, loss of barrier integrity. The prosecretory COPD phenotype was associated with the predominant reduction in multiciliated cells, disabling the elevator function of the bronchial epithelium as reflected by altered CBF. The induction of detrimental changes by submaximal ZnO doses highlights the

importance of detailed knowledge about prevalent pollutants mimicking daily life exposure.

Our findings were in line with previous reports showing altered multiciliated cells differentiation,[33] depression of CBF[34] and impairment of mucociliary clearance[33] in COPD airways. Whereas the prosecretory phenotype of the human bronchial epithelium had been demonstrated in asthma[35] or cystic fibrosis,[36] the phenomenon remained poorly studied in COPD. The prosecretory phenotype in end-stage COPD is likely further promoted by exposure to cigarette smoke and corticosteroids,[33] and may demonstrate adaptive strategies of the airway epithelium that responds to injury with epithelial inflammation,[37] goblet cell expansion, multiciliated cell impairment and EMT.[15 38] The subsequent decrease in barrier function promotes transmigration

of non-infectious (eg, NPs) or infectious (eg, bacteria, fungi) agents.[15]

The use of a state-of-the-art aerosol-cell exposure system (VITROCELL CLOUD) allowed for the standardised exposure to occupationally relevant, cytotoxic and proinflammatory NPs. Proving the relevance of our exposure setting, the applied ZnO concentrations induced strain on cellular zinc homoeostasis with an intracellular accumulation of Zn^{2+} complexes resulting in direct intracellular effects. Interestingly, the increased vulnerability of the multiciliated cells to NP exposure was most pronounced in mild disease (COPD-II) and CSE exposure effectively advanced COPD-II derived pHBECs into an end-stage, prosecretory phenotype on CSE.

The 12-fold higher surface-specific inflammogenicity of ZnO particles in animal models as compared with Printex 90 CNPs exposure[39] could explain the lack of changes in cell viability, membrane integrity and cellular composition in the CNP-exposed airway epithelium despite a fourfold higher surface dose. These findings are in accordance with previous studies on Calu-3-based ALI cultures[40] and could partially be explained by enhanced mucus penetration of ZnO, similar to diesel exhaust particles.[39] Longer-term, intracellular CNP accumulation likely conveys metaplasia and induction of cancerous lesions. Our study revealed the activation of transcription factors associated with a prosecretory phenotype (online supplemental table 3), consistent with our observation that secretory cells were less affected by ZnO-NPs. However, the decreased susceptibility towards short-term NP exposure in patients with COPD cannot only be explained by airway-protective effects of mucus production and goblet cell expansion.[41]

Embryologically, the most important cells in the differentiation process of the bronchial epithelium are the primary bronchial epithelial cells with a multifaceted role in infectious[42] and non-infectious environmental challenges.[43] The predominance of secretory cells at the expense of multiciliated cell number in end-stage COPD likely reflects the impaired differentiation capacity and exhausted regeneration potential of progenitor cells in the diseased airway epithelium,[44] previously suggested by studies in $PM_{2.5}$ exposed human nasal mucosa[12] and longer-term CSE exposures of COPD-II and COPD-IV pHBEC cultures.[15]

By the use of single-cell analysis, we successfully delineated basal cell fate in serial samples from COPD-IV and non-CLD derived pHBECs and revealed an altered differentiation trajectory of the airway basal cell in patients with COPD underlying the observed prosecretory phenotype. Two previously unidentified subsets of basal cells characterise COPD-IV and non-CLD cultures with an increasingly divergent prevalence over time. Following the hypothesis that secretory cells derive from basal cells but function as progenitor cells for multiciliated cells at the same time, we analysed gene kinetics of the secretory cell population. Indeed, in accordance with the data obtained by IF, $MUC5AC^+$ gene expression steadily increased between ALId0-14. At this time point, corresponding to secretory-to-multiciliary cell differentiation,[23] we detected an increase in basal cell abundance, secretory and transitional cells in COPD-IV pHBECs, confirming previous data.[45] Cell frequencies and specific trajectories were validated by systematic comparison with two distinct single-cell datasets of healthy human airways,[25 26] demonstrating high matchScore coefficients, indicating correct generation of in vivo like cell identities in non-CLD and COPD-IV pHBECs.

Enrichment of Wnt and Notch signalling characterises COPD-IV derived basal_1 cells and their secretory cell progeny in line with the bulk transcriptome data obtained in COPD-IV cultures and previous studies.[29] Exposure to ZnO induced additional enrichment of Wnt-pathway components, thus contributing to the imbalanced secretory-multiciliated cell differentiation in accordance with the previously identified activation of Wnt and TGF-ß signalling through ZnO NP exposure.[31 46] Our findings suggest that NPs trigger gene programmes of basal cell renewal and repair, driving secretory cell survival.[47] Induction of reactive oxygen species and ECM remodelling, enhanced by the interaction of Notch and TGF-ß signalling, likely highlights additional survival strategies in secretory cells,[28] further promoted by the activation of these pathways in basal_1 cells.

Accumulation of transitional cells in the COPD-derived epithelium is reflected by the activation of the ciliary machinery observed in bulk transcriptome data of COPD-IV pHBECs, contrasted by the failed presence of end-differentiated multiciliated cells in these cultures. The predicted activation of transcription factors that trigger prosecretory phenotype cell fate (*SPDEF, FOXO1, IL17C, PPRC1, RELA, LAMC1, IRF3, NRF1, SMAD2/4, SMARCA4*) is in conjunction with a reduction of multiciliated cells and an aberrant expression of genes involved in cilia organisation and movement.[41 48] At the transcriptome level, secretory cell differentiation was reflected by *NF-κB*-dependent *IL17/IL1* pathway activation in ZnO-exposed COPD-IV pHBECs, in line with previous studies addressing the *IL17/IL1ß*-mediated inflammasome activation.[49]

In summary, we used a physiological, long-term 3D pHBEC culture model of healthy and diseased bronchial epithelial cells at the ALI to obtain a realistic simulation of the pathophysiological changes provoked by environmental NP exposure. We carefully validated our state-of-the-art in vitro model that confirmed benchmark results[22 50] by in situ (tissue sections) and ex vivo (bronchial punches) data. Certain limitations could be addressed in future studies including the effect of long-term application of systemic glucocorticoids, which might impair cell differentiation to a yet undefined extent. Further, transitional cell states need to be addressed in cell culture systems by antibody staining with the potential to explain the observed differences in total cell number between the two isolation protocols, while characteristic cell ratios remained.

The secretory cells' resilience towards airborne irritant-induced injury likely promotes their positive selection culminating in the clinical symptoms of end-stage COPD patients, aggravated by the predominant loss of multiciliated cells on toxin exposure. Moreover, the presence of an altered basal cell state drives the pathological shift in secretory-multiciliary differentiation, thereby closing the self-perpetuating circle of secretory cell progeny and survival and potentially adding to the non-reversibility of COPD airway pathology. Future therapeutic approaches could aim at modifying secretory cell resilience and basal cell differentiation potential, whereas preventive strategies need to combat disease progression in COPD and the increased risk for cancerous lesions through persistence of pro-oxidative substances such as CNP in the injured airway epithelium.

Author affiliations
[1]Division for Thoracic Surgery Munich, Ludwig-Maximilians-University of Munich (LMU) and Asklepios Medical Center, Munich, , Germany
[2]Institute for Lung Health and Immunity and Comprehensive Pneumology Center with the CPC-M bioArchive, Helmholtz Zentrum Munich, Member of the German Lung Research Center (DZL), Munich, Germany
[3]Department of Medicine V, University Hospital, LMU Munich and Asklepios Medical Center, Munich, Germany
[4]Department of Visceral and Thoracic Surgery Salzburg, Paracelsus Medical University, Salzburg, Austria
[5]Department of Pathology, Asklepios Medical Center, Munich, Germany
[6]Helmholtz Zentrum München – German Research Center for Environmental Health (GmbH), Institute of Experimental Genetics, Neuherberg, Germany

[7]German Center for Diabetes Research (DZD), Neuherberg, Germany
[8]School of Life Sciences, Chair of Experimental Genetics, Technical University Munich, Freising, Germany
[9]Department of Medicine, Pulmonary, Allergy and Critical Care Medicine, University of Pittsburgh, Pittsburgh, Pennsylvania, USA
[10]Department of Mathematics, Technische Universität München, Garching bei München, München, Germany
[11]Metabolomics and Proteomics Core, Helmholtz Center Munich, German Research Center for Environmental Health GmbH, Neuherberg, Germany
[12]Center for Comprehensive Developmental Care at the iSPZ Hauner, Dr. von Haunersches Children's University Hospital, Ludwig-Maximilians-University of Munich (LMU); Member of the German Lung Research Center (DZL), Munich, Germany

Correction notice This article has been corrected since it was published Online First. Author name, equal contributions statement and corresponding author details have been updated.

X Herbert B Schiller @SchillerLab

Contributors AH, HBS, AS, MGS, TS and OS conceived and initiated the study. AH and MGS designed the study. MGS, MS, JJS, CV, YD and MH designed and performed experiments. RAH, CS, JF and ML performed the surgical work. MI and JB performed the transcriptome analysis. AC and BS performed the analysis of the ciliary velocity. SMH performed, analysed and interpreted the secretome data. BS assisted the analysis of secretome and transcriptome data. MA and MS performed the single-cell analysis and interpreted the single-cells data. BS, RAH, JB, TK, OE, TS, OS, AH and HBS analysed and interpreted the results. MH and JJS performed the IF stainings of the native bronchial tissue and primary human bronchial epithelial cells. JJS performed the CSE exposure experiments. MG and GB set up the IF method for the bronchial punches and AS the isolation, culture, differentiation and IF methods for primary human bronchial epithelial cells. ES-P performed the HandE stainings and analysed all IF stainings. MGS and JJS performed the long-term culture of the primary human bronchial epithelial cells. OS, YD and CV designed, implemented and performed aerosol-cell exposure experiments with the ALICE-CLOUD. MGS, MA, MH, HBS and AH designed the figures. MGS drafted and wrote the manuscript. MGS, AH, MA, TS, OS and HBS edited and revised the manuscript. All authors read the final version of the manuscript and interpreted the results. The corresponding author (guarantor of the manuscript content) attests that all listed authors meet authorship criteria.

Competing interests None declared.

Patient consent for publication Consent obtained directly from patient(s).

Ethics approval This study involves human participants and the study was approved by the local ethics committee (LMU, CPC-M bioArchive, 333-10) and written informed consent was obtained from all patients. Participants gave informed consent to participate in the study before taking part.

Provenance and peer review Not commissioned; externally peer reviewed.

Data availability statement Data are available on reasonable request. Data are available on reasonable request (scRNA-seq and transcriptome data were submitted to the NCBI GEO database, accession number GSE233145 and GSE208662).

Supplemental material This content has been supplied by the author(s). It has not been vetted by BMJ Publishing Group Limited (BMJ) and may not have been peer-reviewed. Any opinions or recommendations discussed are solely those of the author(s) and are not endorsed by BMJ. BMJ disclaims all liability and responsibility arising from any reliance placed on the content. Where the content

ORCID iDs
Mircea Gabriel Stoleriu http://orcid.org/0000-0002-1288-809X
Motaharehsadat Heydarian http://orcid.org/0000-0003-4411-5371
Alejandra Castelblanco http://orcid.org/0000-0002-1147-758X
Stefanie M Hauck http://orcid.org/0000-0002-1630-6827

REFERENCES

1 Kido T, Tamagawa E, Bai N, *et al*. Particulate matter induces translocation of IL-6 from the lung to the systemic circulation. *Am J Respir Cell Mol Biol* 2011;44:197–204.
2 Xu X, Ha SU, Basnet R. A review of epidemiological research on adverse neurological effects of exposure to ambient air pollution. *Front Public Health* 2016;4:157.
3 Greenberg MI, Vearrier D. Metal fume fever and polymer fume fever. *Clin Toxicol (Phila)* 2015;53:195–203.
4 Maier KL, Alessandrini F, Beck-Speier I, *et al*. Health effects of ambient particulate matter--biological mechanisms and inflammatory responses to in vitro and in vivo particle exposures. *Inhal Toxicol* 2008;20:319–37.
5 Hansel NN, McCormack MC, Kim V. The effects of air pollution and temperature on COPD. *COPD* 2016;13:372–9.
6 Hegab AE, Nickerson DW, Ha VL, *et al*. Repair and regeneration of tracheal surface epithelium and submucosal glands in a mouse model of hypoxic-ischemic injury. *Respirology* 2012;17:1101–13. 10.1111/j.1440-1843.2012.02204.x Available: https://onlinelibrary.wiley.com/toc/14401843/17/7
7 Chen J-K, Ho C-C, Chang H, *et al*. Particulate nature of inhaled zinc oxide nanoparticles determines systemic effects and mechanisms of pulmonary inflammation in mice. *Nanotoxicology* 2015;9:43–53.
8 Zhao J, Li M, Wang Z, *et al*. Role of Pm2.5 in the development and progression of COPD and its mechanisms. *Respir Res* 2019;20:120.
9 Ling SH, McDonough JE, Gosselink JV, *et al*. Patterns of retention of particulate matter in lung tissues of patients with COPD: potential role in disease progression. *Chest* 2011;140:1540–9.
10 Yuan X, Zhang X, Sun L, *et al*. Cellular toxicity and immunological effects of carbon-based Nanomaterials. *Part Fibre Toxicol* 2019;16.
11 Shi L, Zanobetti A, Kloog I, *et al*. Low-concentration Pm2.5 and mortality: estimating acute and chronic effects in a population-based study . *Environ Health Perspect* 2016;124:46–52.
12 Montgomery MT, Sajuthi SP, Cho S-H, *et al*. Genome-wide analysis reveals mucociliary remodeling of the nasal airway epithelium induced by urban Pm2.5 . *Am J Respir Cell Mol Biol* 2020;63:172–84.
13 Macosko EZ, Basu A, Satija R, *et al*. Highly parallel genome-wide expression profiling of individual cells using nanoliter droplets. *Cell* 2015;161:1202–14.
14 Schamberger AC, Mise N, Jia J, *et al*. Cigarette smoke-induced disruption of bronchial epithelial tight junctions is prevented by transforming growth factor-B. *Am J Respir Cell Mol Biol* 2014;50:1040–52.
15 Schamberger AC, Staab-Weijnitz CA, Mise-Racek N, *et al*. Cigarette smoke alters primary human bronchial epithelial cell differentiation at the air-liquid interface. *Sci Rep* 2015;5:8163.
16 Lenz A-G, Stoeger T, Cei D, *et al*. Efficient bioactive delivery of aerosolized drugs to human pulmonary epithelial cells cultured in air-liquid interface conditions. *Am J Respir Cell Mol Biol* 2014;51:526–35.
17 Srinivasan B, Kolli AR, Esch MB, *et al*. TEER measurement techniques for in vitro barrier model systems. *SLAS Technology* 2015;20:107–26.
18 Smith CM, Djakow J, Free RC, *et al*. ciliaFA: a research tool for automated, high-throughput measurement of ciliary beat frequency using freely available software. *Cilia* 2012;1:14.
19 Ziegenhain C, Vieth B, Parekh S, *et al*. Comparative analysis of single-cell RNA sequencing methods. *Mol Cell* 2017;65:631–43.
20 Angelidis I, Simon LM, Fernandez IE, *et al*. An Atlas of the aging lung mapped by single cell transcriptomics and deep tissue proteomics. *Nat Commun* 2019;10:963.
21 Grade S, Thomas J, Zarb Y, *et al*. Brain injury environment critically influences the connectivity of transplanted neurons. *Sci Adv* 2022;8:23.
22 Raman T, O'Connor TP, Hackett NR, *et al*. Quality control in microarray assessment of gene expression in human airway epithelium. *BMC Genomics* 2009;10:493.
23 Ruiz García S, Deprez M, Lebrigand K, *et al*. Novel dynamics of human mucociliary differentiation revealed by single-cell RNA sequencing of nasal epithelial cultures. *Development* 2019;146:20.

24 Garcia SR, Deprez M, Lebrigand K, *et al*. Single-cell RNA sequencing reveals novel cell differentiation Dynamics during human airway epithelium regeneration. *Cell Biology* [Preprint] 2018.

25 Deprez M, Zaragosi L-E, Truchi M, *et al*. A single-cell Atlas of the human healthy Airways. *Am J Respir Crit Care Med* 2020;202:1636–45.

26 Goldfarbmuren KC, Jackson ND, Sajuthi SP, *et al*. Dissecting the cellular specificity of smoking effects and Reconstructing lineages in the human airway epithelium. *Nat Commun* 2020;11:2485.

27 Chow C-M, Georgiou A, Szutorisz H, *et al*. Variant Histone H3.3 marks promoters of transcriptionally active genes during mammalian cell division. *EMBO Rep* 2005;6:354–60.

28 Tsao P-N, Vasconcelos M, Izvolsky KI, *et al*. Notch signaling controls the balance of ciliated and secretory cell fates in developing airways. *Development* 2009;136:2297–307.

29 Carlier FM, Dupasquier S, Ambroise J, *et al*. Canonical WNT pathway is activated in the airway epithelium in chronic obstructive pulmonary disease. *EBioMedicine* 2020;61:103034.

30 Kneidinger N, Yildirim AÖ, Callegari J, *et al*. Activation of the WNT/Β-Catenin pathway attenuates experimental emphysema. *Am J Respir Crit Care Med* 2011;183:723–33.

31 Meng J, Yang J, Pan T, *et al*. Zno nanoparticles promote the malignant transformation of colorectal epithelial cells in Apcmin/+ mice. *Environ Int* 2022;158:106923.

32 Li R, Zhou R, Zhang J. Function of Pm2.5 in the pathogenesis of lung cancer and chronic airway inflammatory diseases. *Oncol Lett* 2018;15:7506–14.

33 Gohy S, Carlier FM, Fregimilicka C, *et al*. Altered generation of ciliated cells in chronic obstructive pulmonary disease. *Sci Rep* 2019;9:17963.

34 Yaghi A, Zaman A, Cox G, *et al*. Ciliary beating is depressed in nasal cilia from chronic obstructive pulmonary disease subjects. *Respir Med* 2012;106:1139–47.

35 Stewart CE, Torr EE, Mohd Jamili NH, *et al*. Evaluation of differentiated human bronchial epithelial cell culture systems for asthma research. *J Allergy (Cairo)* 2012;2012:943982.

36 Hewson CK, Capraro A, Wong SL, *et al*. Novel antioxidant therapy with the immediate precursor to glutathione, Γ-Glutamylcysteine (GGC), ameliorates LPS-induced cellular stress in in vitro 3d-differentiated airway model from primary cystic fibrosis human bronchial cells. *Antioxidants* 2020;9:1204.

37 Maestrelli P, Saetta M, Mapp CE, *et al*. Remodeling in response to infection and injury. airway inflammation and hypersecretion of mucus in smoking subjects with chronic obstructive pulmonary disease. *Am J Respir Crit Care Med* 2001;164(10 Pt 2):S76–80.

38 Lam HC, Cloonan SM, Bhashyam AR, *et al*. Histone deacetylase 6-mediated selective autophagy regulates COPD-associated cilia dysfunction. *J Clin Invest* 2020;130:143863.

39 Schmid O, Stoeger T. Surface area is the biologically most effective dose metric for acute nanoparticle toxicity in the lung. *J Aerosol Sci* 2016;99:133–43.

40 Turdalieva A, Solandt J, Shambetova N, *et al*. Bioelectric and morphological response of liquid-covered human airway epithelial Calu-3 cell Monolayer to periodic deposition of colloidal 3-mercaptopropionic-acid coated Cdse-CDs/Zns core-multishell quantum dots. *PLoS One* 2016;11:e0149915.

41 Chen G, Korfhagen TR, Karp CL, *et al*. Foxa3 induces goblet cell metaplasia and inhibits innate antiviral immunity. *Am J Respir Crit Care Med* 2014;189:301–13.

42 Ruffin M, Roussel L, Maillé É, *et al*. Vx-809/Vx-770 treatment reduces inflammatory response to pseudomonas aeruginosa in primary differentiated cystic fibrosis bronchial epithelial cells. *Am J Physiol Lung Cell Mol Physiol* 2018;314:L635–41.

43 Ji J, Ganguly K, Mihai X, *et al*. Exposure of normal and chronic bronchitis-like mucosa models to aerosolized carbon nanoparticles: comparison of pro-inflammatory oxidative stress and tissue injury/repair responses. *Nanotoxicology* 2019;13:1362–79.

44 Staudt MR, Buro-Auriemma LJ, Walters MS, *et al*. Airway basal stem/progenitor cells have diminished capacity to regenerate airway epithelium in chronic obstructive pulmonary disease. *Am J Respir Crit Care Med* 2014;190:955–8.

45 Duclos GE, Teixeira VH, Autissier P, *et al*. Characterizing smoking-induced transcriptional heterogeneity in the human bronchial epithelium at single-cell resolution. *Sci Adv* 2019;5:12.

46 Pan C-H, Liu W-T, Bien M-Y, *et al*. Effects of size and surface of zinc oxide and aluminum-doped zinc oxide nanoparticles on cell viability inferred by proteomic analyses. *Int J Nanomedicine* 2014;9:3631–43.

47 Liu Y, Zhou T, Sun L, *et al*. The effect of notch signal pathway on Pm2.5-induced Muc5Ac in Beas-2B cells. *Ecotoxicol Environ Saf* 2020;203:110956.

48 Danahay H, Pessotti AD, Coote J, *et al*. Notch2 is required for inflammatory cytokine-driven goblet cell metaplasia in the lung. *Cell Rep* 2015;10:239–52.

49 Fujisawa T, Velichko S, Thai P, *et al*. Regulation of airway Muc5Ac expression by IL-1Beta and IL-17A; the NF-kappaB paradigm. *J Immunol* 2009;183:6236–43.

50 Rayner RE, Makena P, Prasad GL, *et al*. Optimization of normal human bronchial epithelial (NHBE) cell 3d cultures for in vitro lung model studies. *Sci Rep* 2019;9:500.

51 Ambroz F, Macdonald TJ, Martis V, *et al*. Evaluation of the BET theory for the characterization of meso and microporous mofs. *Small Methods* 2018;2:11. 10.1002/smtd.201800173 Available: https://onlinelibrary.wiley.com/toc/23669608/2/11